Monthly Notices of the ROYAL ASTRONOMICAL SOCIETY

MNRAS **513,** 5567–5574 (2022) https://doi.org/10.1093/mnras/stac1208
Advance Access publication 2022 April 30

SXP 15.6 – an accreting pulsar close to spin equilibrium?

M. J. Coe [1★] I. M. Monageng [2,3] J. A. Kennea [4] D. A. H. Buckley [2] P. A. Evans [5] A. Udalski,[6] Paul Groot,[2,7,8] Steven Bloemen,[7] Paul Vreeswijk,[7] Vanessa McBride,[9] Marc Klein-Wolt,[7] Patrick Woudt,[8] Elmar Körding,[7] Rudolf Le Poole[10] and Danielle Pieterse[7]

[1]*Physics & Astronomy, The University of Southampton, Southampton SO17 1BJ, UK*
[2]*South African Astronomical Observatory, PO Box 9, Observatory, Cape Town 7935, South Africa*
[3]*Department of Astronomy, University of Cape Town, Private Bag X3, Rondebosch 7701, South Africa*
[4]*Department of Astronomy and Astrophysics, The Pennsylvania State University, 525 Davey Lab, University Park, PA 16802, USA*
[5]*Astrophysics Group, School of Physics & Astronomy, University of Leicester, University Road, Leicester LE1 7RH, UK*
[6]*Astronomical Observatory, University of Warsaw, Al. Ujazdowskie 4, P-00-478 Warszawa, Poland*
[7]*Department of Astrophysics/IMAPP, Radboud University, PO Box 9010, NL-6500 GL Nijmegen, the Netherlands*
[8]*Department of Astronomy & Inter-University Institute for Data Intensive Astronomy, University of Cape Town, Private Bag X3, Rondebosch 7701, South Africa*
[9]*IAU – Office of Astronomy for Development, PO Box 9, Observatory 7935, South Africa*
[10]*Leiden Observatory, Leiden University, PO Box 9513, NL-2300 RA Leiden, the Netherlands*

Accepted 2022 April 25. Received 2022 April 19; in original form 2022 March 7

ABSTRACT

SXP 15.6 is a recently established Be star X-ray binary system in the Small Magellanic Cloud (SMC). Like many such systems, the variable X-ray emission is driven by the underlying behaviour of the mass donor Be star. It is shown here that the neutron star in this system is exceptionally close to spin equilibrium averaged over several years, with the angular momentum gain from mass transfer being almost exactly balanced by radiative losses. This makes SXP 15.6 exceptional compared to all other known members of its class in the SMC, all of whom exhibit much higher spin period changes. In this paper, we report on X-ray observations of the brightest known outburst from this system. These observations are supported by contemporaneous optical and radio observations, as well as several years of historical data.

Key words: stars: emission line, Be – X-rays: binaries.

1 INTRODUCTION

Be star X-ray binary systems (BeXRBs) are a large sub-group of the well-established category of high-mass X-ray binaries (HMXBs) characterized by being a binary system consisting of a massive mass donor star, normally an OBe type, and an accreting compact object, a neutron star (though there is one known system, MWC 656, where the accretor is a black hole; Casares et al. 2014). The Small Magellanic Cloud (SMC) has been known for quite a while now to contain the largest known collection of BeXRBs – see e.g. Coe & Kirk (2015) and Haberl & Sturm (2016). Despite the many observational studies, it remains clear that the complex interactions between the two stars continue to produce unexpected surprises. In particular, the unpredictable behaviour of the mass donor OB-type star is a major driver in the observed characteristics of such systems, and as a direct result of the rate of mass transfer on to the neutron star systems long-term spin-up or spin-down changes are observed (Klus et al. 2014).

It is rare to find a system that approaches long-term equilibrium and an essentially zero spin period change. The source that is the subject of this paper, SXP 15.6, could be such a system and was identified as a BeXRB by Vasilopoulos et al. (2017). The optical counterpart [M2002] SMC 12102 is proposed to have a similar spectral type by several authors: O9.5Ve by Evans et al. (2004), O9IIIe by Lamb et al. (2016), and B0IV-Ve by McBride et al. (2017).

Reported here are multiwaveband observations covering the X-ray and optical bands over several years showing the pattern of changes seen in this system. There are three broad occasions when SXP 15.6 was detected by the SMC X-ray survey project S-CUBED (Kennea et al. 2018) for a period of several hundred days, with the most recent detection (2021 November) being the brightest so far seen. In particular, it is noted that the pulse period change over several years is shown to be extremely small for such a BeXRB system.

2 OBSERVATIONS

2.1 X-rays – S-CUBED

SXP 15.6 was detected by the S-CUBED survey (Kennea et al. 2018), a shallow weekly X-ray survey of the optical extent of the SMC by the *Swift* X-ray Telescope (XRT; Burrows et al. 2005). Individual exposures in the S-CUBED survey are typically 60 s long, and occur weekly, although interruptions can occur due to scheduling constraints. Full details of the X-ray reduction and manner in which sources are identified and their fluxes quantified can be found in Kennea et al. (2018).

★ E-mail: mjcoe@soton.ac.uk

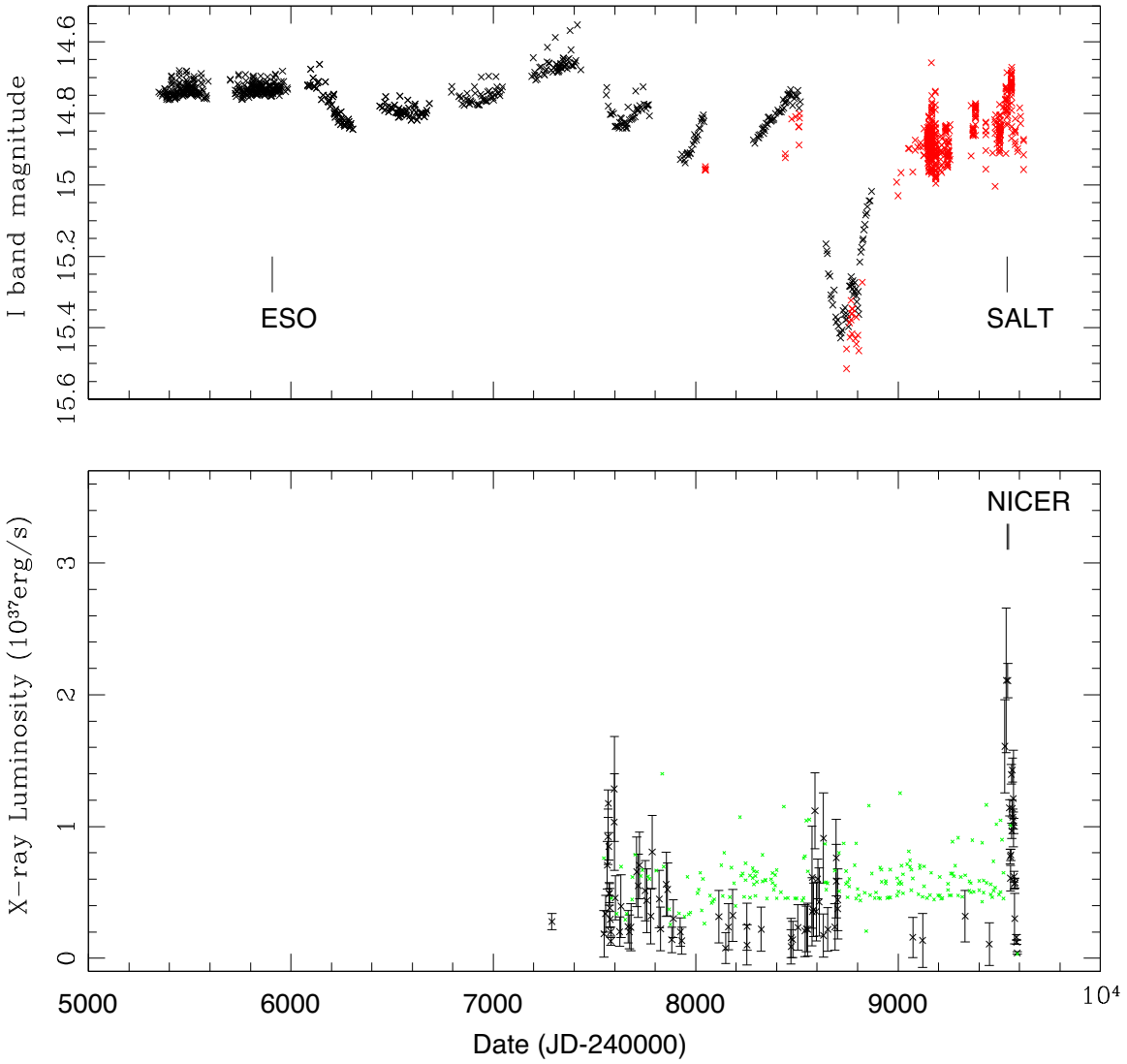

Figure 1. Long-term S-CUBED X-ray (lower panel) and *I*-band (upper panel) detections. The *I* band is a composite of OGLE IV *I*-band data (in black) and MeerLICHT *i*-band observations (in red). Note that MeerLICHT values have been adjusted for the slight differences in band passes (see the text). The green points in the lower panel indicate 90 per cent X-ray upper limits from non-detections. The dates of the ESO, SALT, and NICER observations are indicated.

SXP 15.6 was first detected by the S-CUBED observation taken on MJD 57547 (2016 June 6) and reported by Evans, Kenna & Coe (2016). It has been seen many times since then (see Fig. 1). There have been a total of 280 S-CUBED observations over the ∼6 yr period (91 detections and 189 upper limits); the results are shown in Fig. 1. It is noticeable that there have been three distinct periods of X-ray activity over these ∼5 yr, with the most recent one being the X-ray brightest (Coe et al. 2021). A detailed plot of the most recent outburst is shown in Fig. 2, which shows that, at its peak, the XRT count rate was 0.56 ± 0.05 cts s^{-1}. Using a standard SMC distance of 62 kpc (Scowcroft et al. 2016) and correcting for absorption fixed at the value derived from Willingale et al. (2013), this corresponds to a peak 0.3–10 keV luminosity of $(1.8 \pm 0.2) \times 10^{37}$ erg s^{-1}.

2.2 X-rays – NICER

Follow-up observations were carried out by the Neutron Star Interior Composition Explorer (NICER) (Arzoumanian & Gendreau 2016). A NICER 7.3 ks observation for SXP 15.6 was obtained beginning 02:04 UT on 2021 November 20 and the results first reported by Coe et al. (2021) who revealed the presence of a significant detection of the pulsar period at 15.640 34(1) s based on the first NICER observation. This same pulsar period was also weakly detected in the *Swift* XRT data.

In order to more accurately measure the spin period and evolution of the pulsar, we have analysed the first 7 d of NICER observations, in which the source was both bright and densely observed, with eight observations being taken between 2021 November 20 and 2021 November 27, representing a total of 31.6 ks of observations during that time period.

These data were processed using the standard HEASOFT 6.30 tools,[1] with barycentric corrections applied using the `barycorr` tool. A photon time of arrival (TOA) analysis was performed, in order to accurately measure the pulsar frequency and derivatives over

[1]NASA High Energy Astrophysics Science Archive Research Center (HEASARC) (2014).

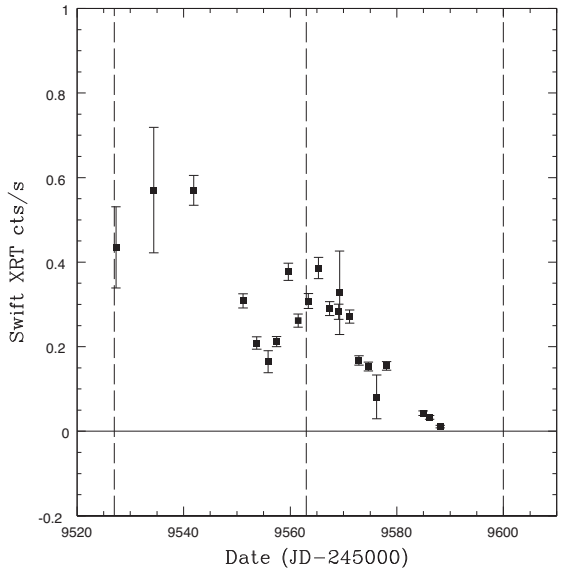

Figure 2. *Swift* XRT data during the current outburst (2021 November). The vertical dashed lines indicate the predicted time of optical outbursts given by equation (2).

Table 1. Pulsar timing parameters for SXP 15.6 based on the first 7 d of NICER observations.

Parameter	Value
Epoch (MJD)	59 538.087
f (Hz)	0.063 939 66(9) Hz
$\dot{f}$ (Hz s^{-1})	$(6.544 \pm 0.819) \times 10^{-12}$
$\ddot{f}$ (Hz s^{-2})	$-1.382 \pm 0.292 \times 10^{-17}$

this period of intense monitoring. This TOA analysis utilized the NICERsoft[2] tools to perform the required pulse profile modelling, splitting of event data, and TOA analysis. These resultant TOAs were then fit to find the pulsar frequency and its derivatives utilizing the PINT pulsar timing software package (Luo et al. 2021), specially utilizing the `pintk` user interface tool to perform the TOA fit.

Utilizing these tools, it was possible to find a phase-locked period solution to the first 7 d of NICER observations. The resultant frequency fit is given in Table 1, and gives a best-fitting pulsar period of 15.639 743 ± 0.000 022 s. It is noteworthy that this pulsar period is consistent within errors with the value of 15.6398 ± 0.0009 s reported in a 2016 observation by Vasilopoulos et al. (2017), suggesting no strong evolution of the spin period in the last 5 yr.

The NICER-derived value of $\dot{f}$, which equates to a pulsar spin-up $\dot{P}$ of $-1.60 \pm -0.20 \times 10^{-9}$ s s^{-1}, or approximately -0.051 ± 0.06 s yr^{-1} suggests that there is additional spin-up of the pulsar occurring during the X-ray outburst due to accretion. As the implied period derivative between 2016 and 2021 observations ($\dot{P} = -0.12 \pm 2.0 \times 10^{-4}$ s yr^{-1}) is much smaller than this instantaneous value, this suggests that this spin-up is not occurring during periods of quiescence, and only during the short period of outburst.

This lack of change in the pulse period over 5–6 yr is discussed later.

[2]https://github.com/paulray/NICERsoft

2.3 OGLE IV

The OGLE project (Udalski, Szymański & Szymański 2015) provides long-term *I*-band photometry with a cadence of 1–3 d. The star [M2002] SMC 12102 was observed continuously for over a decade until COVID-19 restrictions prevented any further observations after 2020 March. It is identified in the OGLE catalogue as

OGLE IV (*I* band): SMC720.11.13342

OGLE IV (*V* band): SMC720.11.20699v

The *I*-band light curve produced from the OGLE IV observations is shown in Fig. 1.

2.4 MeerLICHT

[M2002] SMC 12102 was monitored with the MeerLICHT telescope using SDSS filters (u, g, r, i, z) and a wider q-band filter (4400−7200 Å) at 60 s integration time for each filter. MeerLICHT is a prototype of the Black GEM array (Groot 2019) and is primarily built to provide simultaneous sky coverage as the MeerKAT radio telescope. The telescope comprises a 0.65 m primary mirror with a 110 megapixel CCD, resulting in a 2.7 deg^2 field of view (Bloemen et al. 2016). The MeerLICHT images were processed with the BlackBOX pipeline (Vreeswijk & Paterson 2021), which carries out primary reductions that include bias subtraction, overscan corrections, and flat-fielding. The subsequent steps performed by the pipeline include astrometric calibration, estimation of the point spread function as a function of position, and photometric calibration.

To complement the OGLE coverage and to fill the gap after OGLE IV ended, the MeerLICHT *i*-band data have been added to Fig. 1. However, because the band passes for Johnson *I* and Sloan *i* are slightly different, the MeerLICHT results have been adjusted according to the transformations given by Jordi, Grebel & Ammon (2006). As a result, the MeerLICHT values were adjusted by an amount of −0.31 mag for display in this figure.

The unmodified light curves from the MeerLICHT *u*-, *q*-, and *i*-band filters are shown in Fig. 3. It is apparent from the figure that it is the red colour that changes most over time, indicative of the variable nature of the light from the circumstellar disc that is cooler, in general, than the star. This is quantified by comparing the size of the brightness decrease seen in all the filters around MJD 58800 compared to MJD 59200 (see Table 2). Note though SXP 15.6 was measured at the time of its faintest state in all filters, the general coverage in the g, r, and z bands is sparse, so is not shown in Fig. 3.

2.5 SALT and ESO spectra

[M2002] SMC 12102 was observed with the ESO Faint Object Spectrograph and Camera v2 (EFOSC2 Buzzoni et al. 1984), mounted at the Nasmyth B focus of the 3.6m New Technology Telescope (NTT) at La Silla Observatory, Chile, on the night of 2011 December 11 (TJD 55907).The instrument was in long-slit mode with a slit width of 1.5 arcsec and instrument binning 2 × 2. Grism 20 was used to obtain spectra at (∼6000–7000 Å) wavelengths. For Grism 20, this lead to a dispersion of ∼1 Å pix^{-1} and a resolution of ∼6 Å per full width at half-maximum. The spectra were reduced, extracted, and calibrated using the standard IRAF[3] packages.

[M2002] SMC 12102 was also observed with the Southern African Large Telescope (SALT; Buckley, Swart & Meiring 2006) using the Robert Stobie Spectrograph (Burgh et al. 2003; Kobulnicky et al.

[3]Image Reduction and Analysis Facility: iraf.noao.edu.

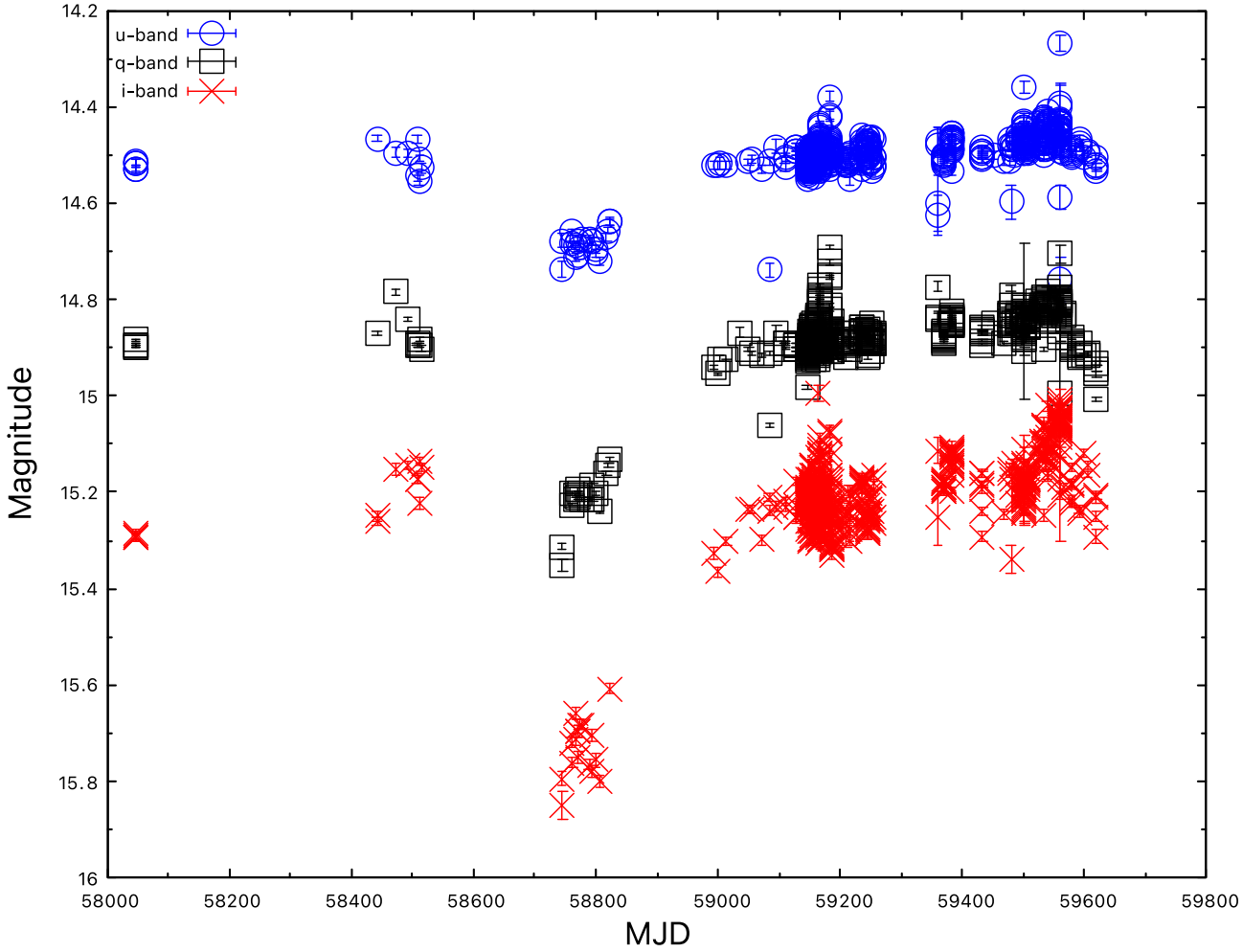

Figure 3. MeerLICHT *u*- (blue open circles), *q*- (black open squares), and *i*-band (red crosses) light curves.

Table 2. Table of maximum brightness decrease in SXP 15.6 seen by MeerLICHT.

Waveband	Wavelength range (Å)	Δm
u	3400–4100	0.20 ± 0.05
g	4100–5500	0.22 ± 0.05
r	5600–6900	0.35 ± 0.05
q	4400–7200	0.45 ± 0.05
i	6900–8400	0.55 ± 0.05
z	8400–10 000	0.50 ± 0.05

2003) on 2021 November 19 (MJD59538) and 2021 December 8 (MJD59557). The PG2300 grating was used with an exposure time of 1200 s covering a wavelength range 6100–6900 Å. The SALT science pipeline (Crawford et al. 2012) was used to perform primary reductions, which include overscan corrections, bias subtraction, gain and amplifier cross-talk corrections. The remaining steps, comprising wavelength calibration, background subtraction, and extraction of the one-dimensional spectrum were executed with IRAF.

The SALT Hα spectra compared to the historic ESO spectrum are shown in Fig. 4. The measured Hα equivalent width values are MJD 55906 $-$ 6.12 $\pm$ 0.31 Å, MJD 59538 $-$ 8.20 $\pm$ 0.30 Å, and MJD 59557 $-$ 9.40 $\pm$ 0.47 Å. This indicates a $\sim$50 per cent flux increase in this line between 2011 December and 2021 November.

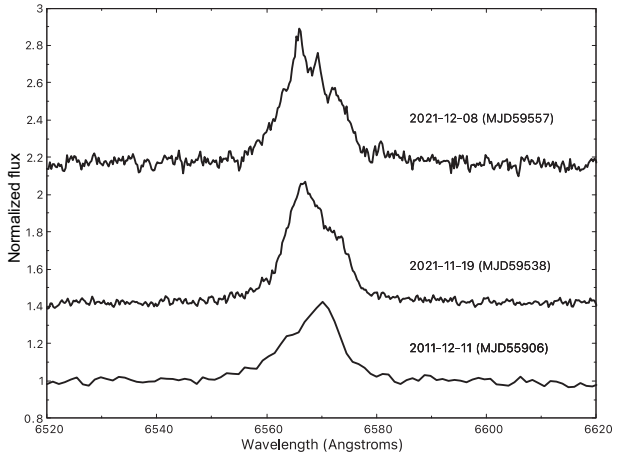

Figure 4. Hα from ESO and SALT-ITU. Hα emission line (bottom is from ESO and top 2 are from SALT).

The most recent line profiles reveal multiple structural features that are only hinted at in the earliest spectrum. Presumably, these features are related to changing structures in the circumstellar disc as it goes through a re-building phase and interacts gravitationally with the orbiting neutron star, thereby triggering the observed X-ray emission.

Table 3. MeerKAT (1.28 GHz) upper limits of SXP 15.6 at the 3σ level.

MJD	Radio flux density (μJy)	Luminosity (erg s^{-1})
59559	<33.9	$<2.0 \times 10^{29}$
59563	<32.7	$<1.9 \times 10^{29}$
59565	<37.5	$<2.2 \times 10^{29}$
59566	<30.6	$<1.8 \times 10^{29}$

2.6 MeerKAT

We observed SXP 15.6 with the MeerKAT radio array (Jonas 2009) during the current outburst at a central frequency of 1.28 GHz for four epochs. The observations were done with a bandwidth of 856 MHz, with the correlator configured to deliver 4096 channels. Each observation consisted of 1 h scans of the target and 2 min scans of the phase calibrator J0252−7104. We used J0408−6545 as the primary calibrator, which was observed at the start and end of each observation for 5 min. We processed the data with the Oxkat (Heywood 2020) reduction routines. Oxkat contains scripts that average the data to 1024 channels, applies standard bandpass and gain corrections, followed by flagging of the data. The target field was then imaged using WSCLEAN, and then a process of self-calibration was executed using CUBICAL. All the images resulted in a non-detection at the optical position of SXP 15.6 (∼1 arcsec positional error). The 3σ upper limits are given in Table 3. In Fig. 5, we plot the 3σ radio luminosity upper limits with the simultaneous X-ray luminosities. In this plot, the MeerKAT flux densities were converted to 6 GHz luminosities by assuming a flat spectrum and using the SMC distance of 62 kpc (Scowcroft et al. 2016). For comparison, we include X-ray and radio luminosity measurements of X-ray binaries from Bahramian et al. (2018) and van den Eijnden et al. (2021).

3 DISCUSSION

3.1 Long-term spin period changes

Klus et al. (2014) published a study of the spin period changes, $P_{\rm dot}$, in 42 BeXRB systems in the SMC. From their results, it is possible to determine the average $P_{\rm dot}$ over more than a decade for these systems (see Fig. 6). Comparing the NICER spin period of SXP 15.6 with that of the *Chandra* measurement in 2016 July (Vasilopoulos et al. 2017), it is possible to determine that the average spin period change over the ∼6 yr is -2.91×10^{-8} s d^{-1} or -1.06×10^{-5} s yr^{-1}. This is an extremely small absolute value of $P_{\rm dot}$, by far the smallest of all the 43 systems so far measured in the SMC. This exceptionally low spin period change is illustrated in Fig. 6.

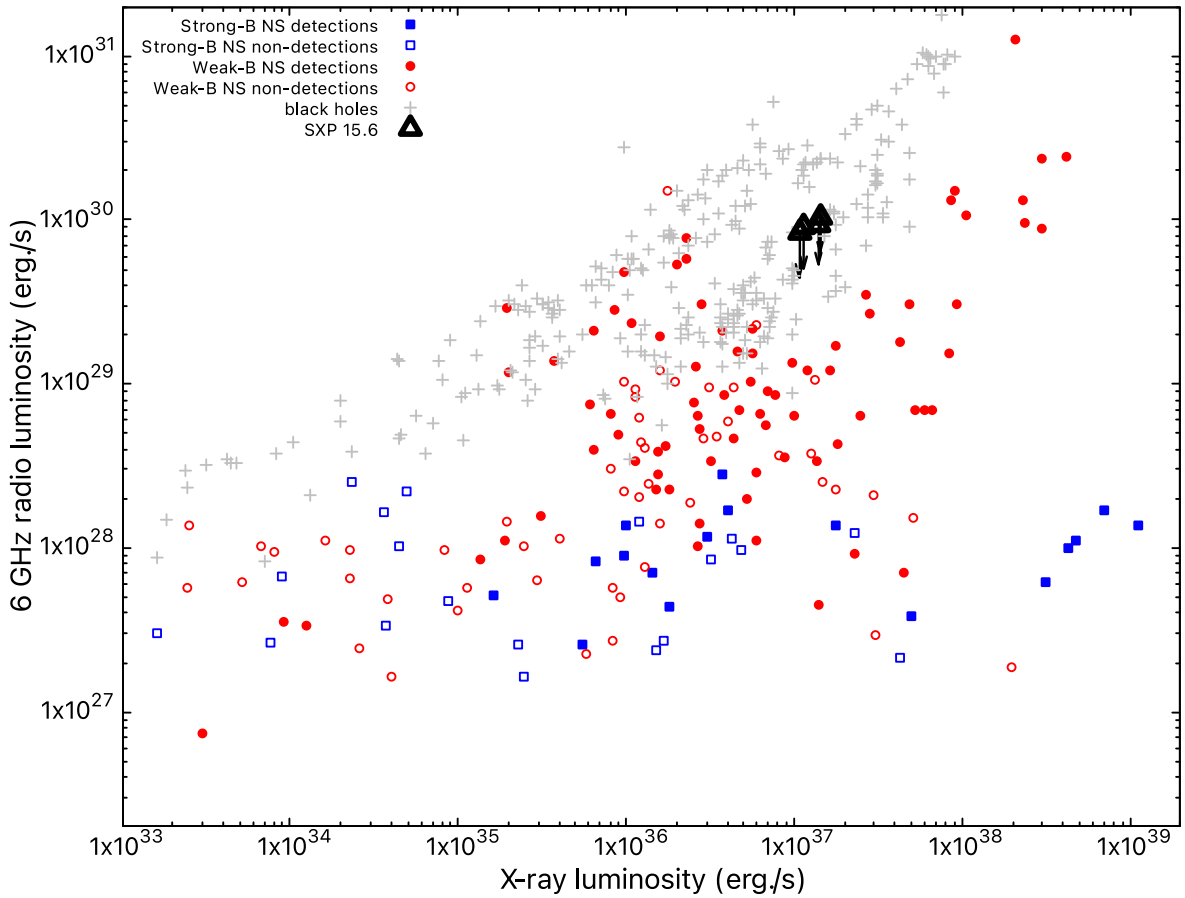

Figure 5. The radio/X-ray correlation for X-ray binaries. The measurements for SXP 15.6 are shown with the triangle symbols. Archival measurements of strongly magnetized and weakly magnetized neutron star systems are shown with the filled squares and circles, respectively. Radio upper limits of the strongly magnetized and weakly magnetized neutron star systems are shown with the open squares and circles, respectively. Archival black holes are shown in grey plus symbols. The archival data in this plot are taken from the X-ray binary data base compiled by Bahramian et al. (2018) and van den Eijnden et al. (2021) (see their fig. 1).

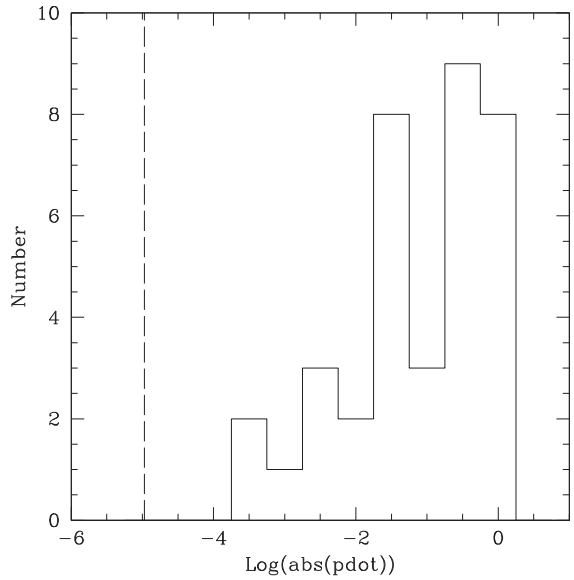

Figure 6. Histogram of log of the absolute value of $P_{\rm dot}$ ($P_{\rm dot}$ in units of s yr^{-1}) for 42 SXP systems averaged over 10 yr (Klus et al. 2014). The vertical dashed line shows the position of SXP 15.6 from this work.

Of all the 43 BeXRB sources currently known in the SMC with spin periods, SXP 15.6 is by far the closest to exhibiting spin equilibrium, at least in the last 6 yr. Klus et al. (2014) review models for accretion on to neutron stars and their equation (18) [based on the work by Davidson & Ostriker (1973)] permits the determination of the neutron star magnetic field under such equilibrium circumstances:

$$B \approx 1.8 \times 10^{13} R^{-3} \left(\frac{M}{M_{\odot}}\right)^{5/6} (\dot{M})^{0.5} \left(\frac{P_{\rm spin}}{100}\right)^{7/6} \ {\rm G}, \qquad (1)$$

where R is the neutron star radius in units of 10^6 cm, M is the mass of the neutron star, $\dot{M}$ is the mass accretion rate in units of 10^{16} g s^{-1}, and $P_{\rm spin}$ is the spin period in seconds.

Normal values are assumed here for the neutron star mass (1.4 $M_{\odot}$) and radius (10 km). The spin period for SXP 15.6 is, of course, 15.6 s. To evaluate $\dot{M}$, it was first necessary to find the average X-ray luminosity from the 280 S-CUBED observations over the ∼6 yr period (91 detections and 189 upper limits). That was found to be 1.7×10^{36} erg s^{-1} – non-detections were assigned an arbitrarily low luminosity value of 10^{33} erg s^{-1}. Using that average luminosity and assuming a mass-to-energy conversion efficiency of 10 per cent gives $\dot{M} = 2.1 \times 10^{16}$ g s^{-1}. Putting that number back into equation (1) results in a predicted magnetic field of 3.7×10^{12} G for the neutron star in SXP 15.6.

3.2 Comparing X-ray with optical light curves

Fig. 1 shows the totality of our optical and X-ray data on SXP 15.6. The OGLE IV *I*-band data have been supplemented with MeerLICHT *i* band. In the figure, the MeerLICHT data have been adjusted by 0.36 mag so that they agree with OGLE IV where they overlap. This is necessary as the two filters used (*I* and *i*) have slightly different bandwidth responses.

A visual inspection of the OGLE IV data in this figure quickly reveals the existence of short optical spikes, predominantly obvious during the period 5346–7772 TJD. Taking that interval of data, detrending it, and then applying a generalized Lomb–Scargle timing

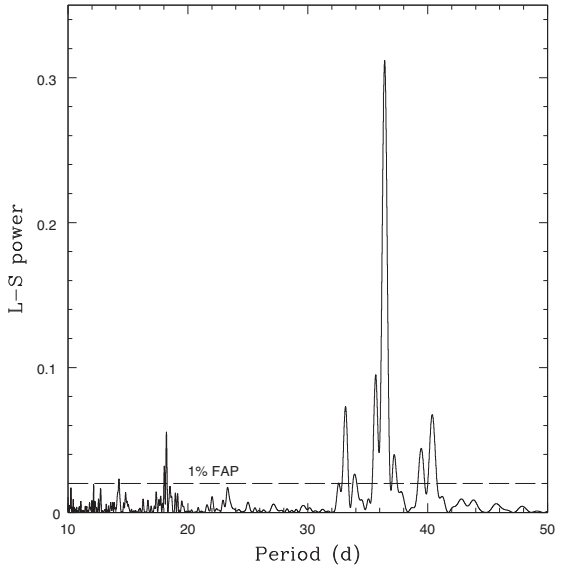

Figure 7. Generalized Lomb–Scargle power spectrum from the OGLE IV data. The peak is at 36.411 d.

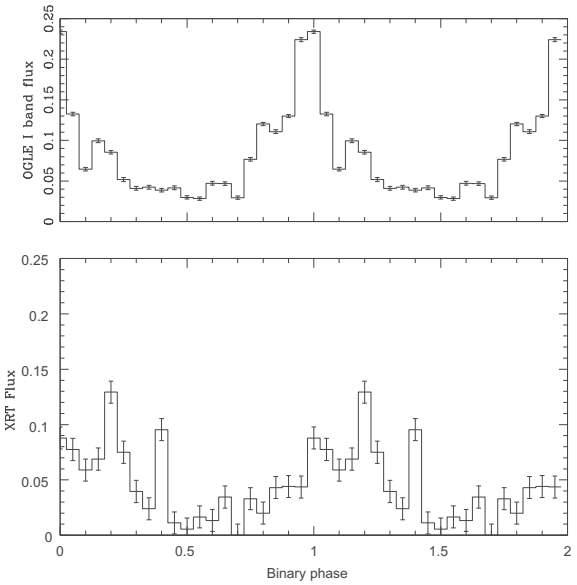

Figure 8. OGLE IV *I*-band data (upper panel) and S-CUBED X-ray data (lower panel) folded at the binary period given in equation (2).

analysis (Zechmeister & Kürster 2009) reveals a strong, clear peak in the power spectrum at a period of 36.411 d (see Fig. 7).

The ephemeris for the time of the optical outbursts, $T_{\rm opt}$, is here updated from the earlier measurements of McBride et al. (2017) and is now given by

$$T_{\rm opt} = 2455376.41 + N(36.411) \ {\rm JD}. \qquad (2)$$

The S-CUBED X-ray flux is compared to the OGLE IV fluxes, both folded with the ephemeris given in equation (2), in Fig. 8. It is immediately clear that the X-ray emission is only weakly correlated with the OGLE modulation, both in width and in peak position. Though the gravitational pull of the arriving neutron star is believed to extend the surface area of the optically thick circumstellar disc, thereby increasing the *I*-band emission, it seems to have little effect

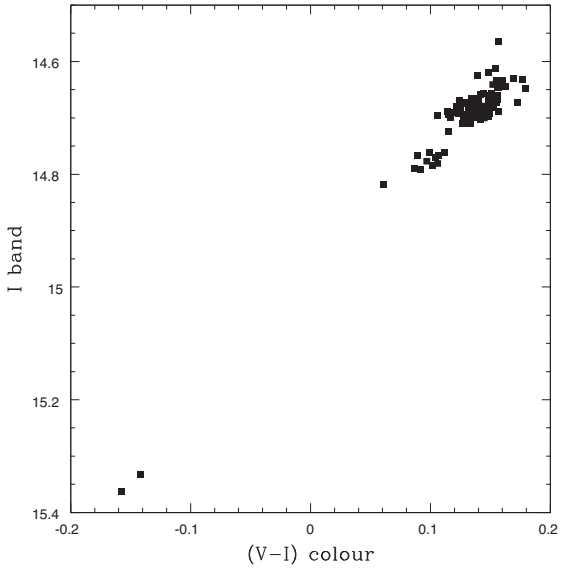

Figure 9. OGLE IV colour–magnitude diagram from data collected over ∼9 yr.

on the material accreting on to the neutron star and triggering X-ray emission. There is some suggestion that the period of X-ray maximum lags the optical peak by a phase of ∼0.2.

More generally, it can be seen from Fig. 1 that the times when the source is most X-ray active are correlated with the source exhibiting its more normal bright state. The dip in the *I* band around TJD 8800 of some 0.7 mag coincides with the period when S-CUBED was failing to detect the system. In contrast, the most recent X-ray bright state around TJD 9500–9600 marks the recovery of the circumstellar disc, and the resultant availability of material for accretion.

3.3 OGLE and MeerLICHT colour–magnitude diagrams

The optical counterpart [M2002] SMC 12102 is proposed to be of spectral type O9.5Ve by Evans et al. (2004), O9IIIe by Lamb et al. (2016), and B0IV-Ve by McBride et al. (2017). The intrinsic $(V-I)$ colour of O9.5V − B0V is in the range of −0.361 to −0.355 in Pecaut & Mamajek (2013). The OGLE dust maps of the SMC (Skowron et al. 2021) enable the precise reddening correction to be made for such an object in the SMC and that is $E(V-I)=0.067$. Thus, the predicted observed colours of [M2002] SMC 12102 if it were a B-type star in this range with no circumstellar disc will be $(V-I) = -0.294$ to −0.288. From Fig. 9, it can be seen that the observed colours are always much redder than this value, even during the epoch when the source was at its faintest for a few years. This strongly suggests the presence of a persistent circumstellar disc, adding further reddening to the observed colours. However, it is worth noting that the system has a clear pattern of being much bluer when fainter, strongly suggesting that all the variations seen in the *I*-band magnitude are due to variations in this disc size.

Figs 9 and 10 reveal a strong correlation between the brightness and colour. This is an indicator of a low/intermediate disc inclination, since the growth results in overall excess brightness and reddening of the system as the outer parts of the disc are cooler than the inner parts. The inference of a low disc inclination is corroborated by the single-peak morphology of the Hα emission line (Fig. 4).

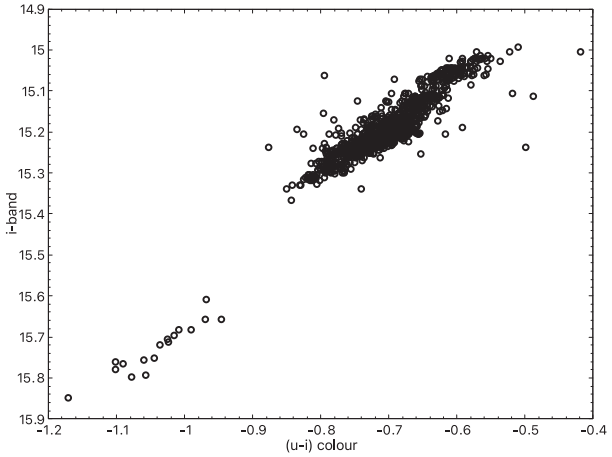

Figure 10. MeerLICHT CMD – data from just the recent outburst epoch.

3.4 Circumstellar disc parameters

To estimate the probable dimensions of the disc and neutron star orbit, some assumptions are needed.

The EW of the Hα emission line may be used as a gauge to the size of the disc and was shown to be correlated to radii measurements from optical interferometry of nearby isolated Be stars (Grundstrom & Gies 2006). Taking the Hα typical value during the recent outburst as -9 ± 1 Å, this predicts an Hα emitting disc of radius 130–280 $R_\odot$ or $(0.9-1.9) \times 10^{11}$ m.

Also assuming, for simplicity, that the neutron star is in a circular orbit, then the period of 36 d permits an estimate of the orbital radius to be 9.0×10^{10} m. That is in good agreement with the estimate for the disc size and, broadly speaking, this is what smooth particle hydrodynamics simulations of such systems predict (Okazaki & Negueruela 2001; Brown et al. 2019). Specifically, the neutron star orbit is constraining further disc expansion beyond that point.

3.5 Radio emission

van den Eijnden et al. (2021) presented a comprehensive study of radio observations of neutron star X-ray binaries. In their work, they demonstrate that strongly magnetized accreting neutron stars ($B \geq 10^{10}$ G), such as those in BeXRBs, can be detected at radio frequencies, contrary to what was previously thought. The Galactic BeXRB systems A0535+262 and *Swift* J0243.6+6124 were detected in the radio during enhanced accretion states that resulted in type II X-ray outbursts (van den Eijnden et al. 2019, 2020). The radio emission in these systems is proposed to be due to the launch of an accretion-powered jet. The non-detection of radio emission from SXP 15.6 during its high X-ray state ($L_X > 10^{37}$ erg s^{-1}) possibly indicates a weak or absent jet. However, because SXP 15.6 is the only extragalactic X-ray binary in Fig. 5, it is only just possible to reach the needed sensitivity to detect the fluxes observed from previously reported galactic systems. It is expected that future radio telescopes in the Southern hemisphere should soon make this goal much more achievable, and the large sample of BeXRB systems in the Magellanic Clouds will be important targets for further understanding of the radio emission from such HMXBs.

4 CONCLUSIONS

BeXRB systems have been known for a long time to show both spin-up and spin-down signatures, depending, it is believed, upon the

average accretion rates of material on to the neutron star. However, the system that is the subject of this paper, SXP 15.6, is demonstrating the closest example yet known where spin equilibrium appears to prevail over the several years it has been studied. Such a system is rare and it provides a valuable example in understanding the panoply of accretion mechanisms that are proposed for these BeXRB systems.

ACKNOWLEDGEMENTS

The OGLE project has received funding from the National Science Centre, Poland, grant MAESTRO 2014/14/A/ST9/00121 to AU. PAE acknowledges UKSA support. JAK acknowledges support from NASA grant NAS5-00136. This work made use of data supplied by the UK Swift Science Data Centre at the University of Leicester.

PJG was supported by NRF SARChI grant 111692.

The MeerLICHT telescope is designed, built, and operated by a consortium consisting of Radboud University, the University of Cape Town, the South African Astronomical Observatory, the University of Oxford, the University of Manchester, and the University of Amsterdam, with support from the South African Radio Astronomy Observatory.

The MeerKAT telescope is operated by the South African Radio Astronomy Observatory, which is a facility of the National Research Foundation, an agency of the Department of Science and Innovation.

IMM, DAHB, VM, and PW were supported by the South African NRF.

Some of the observations reported in this paper were obtained with the Southern African Large Telescope (SALT), as part of the Large Science Programme on transients (2018-2-LSP-001; PI: Buckley).

NICER is a 0.2–12 keV X-ray telescope operating on the International Space Station. The NICER mission and portions of the NICER science team activities are funded by NASA.

DATA AVAILABILITY

All X-ray data are freely available from the NASA *Swift* and NICER archives. The OGLE optical data in this article will be shared on any reasonable request to Andrzej Udalski of the OGLE project. Requests to access the MeerLICHT data should be addressed to Paul Groot.

REFERENCES

Arzoumanian Z., Gendreau K. C., 2016, in AAS/High Energy Astrophysics Division #15. American Astronomical Society, Washington, DC, USA, p.302.01

Bahramian A. et al., 2018, Radio/X-ray correlation database for X-ray binaries. Available at: https://doi.org/10.5281/zenodo.1252036

Bloemen S. et al., 2016, in Hall H. J., Gilmozzi R., Marshall H. K., eds, Proc. SPIE Conf. Ser. Vol. 9906, Ground-Based and Airborne Telescopes VI. SPIE, Bellingham, p. 990664

Brown R. O., Coe M. J., Ho W. C. G., Okazaki A. T., 2019, MNRAS, 488, 387

Buckley D. A. H., Swart G. P., Meiring J. G., 2006, in Stepp L. M., ed., Proc. SPIE Conf. Ser. Vol. 6267, Ground-Based and Airborne Telescopes. SPIE, Bellingham, p. 62670Z

Burgh E. B., Nordsieck K. H., Kobulnicky H. A., Williams T. B., O'Donoghue D., Smith M. P., Percival J. W., 2003, in Iye M., Moorwood A. F. M., eds, Proc. SPIE Conf. Ser. Vol. 4841, Instrument Design and Performance for Optical/Infrared Ground-Based Telescopes. SPIE, Bellingham, p. 1463

Burrows D. N. et al., 2005, Space Sci. Rev., 120, 165

Buzzoni B. et al., 1984, The Messenger, 38, 9

Casares J., Negueruela I., Ribó M., Ribas I., Paredes J. M., Herrero A., Simón-Díaz S., 2014, Nature, 505, 378

Coe M. J., Kirk J., 2015, MNRAS, 452, 969

Coe M. J., Evans P. A., Kennea J. A., Gendreau K., Arzoumanian Z., Ferrara E., Buckley D., Monageng I., 2021, Astron. Telegram, 15054, 1

Crawford S. M. et al., 2012, Astrophysics Source Code Library, record ascl:1207.010

Davidson K., Ostriker J. P., 1973, ApJ, 179, 585

Evans C. J., Howarth I. D., Irwin M. J., Burnley A. W., Harries T. J., 2004, MNRAS, 353, 601

Evans P. A., Kenna J. A., Coe M. J., 2016, Astron. Telegram, 9197, 1

Groot P. J., 2019, Nat. Astron., 3, 1160

Grundstrom E. D., Gies D. R., 2006, ApJ, 651, L53

Haberl F., Sturm R., 2016, A&A, 586, A81

Heywood I., 2020, Astrophysics Source Code Library, record ascl:2009.003

Jonas J. L., 2009, IEEE Proc., 97, 1522

Jordi K., Grebel E. K., Ammon K., 2006, A&A, 460, 339

Kennea J. A., Coe M. J., Evans P. A., Waters J., Jasko R. E., 2018, ApJ, 868, 47

Klus H., Ho W. C. G., Coe M. J., Corbet R. H. D., Townsend L. J., 2014, MNRAS, 437, 3863

Kobulnicky H. A., Nordsieck K. H., Burgh E. B., Smith M. P., Percival J. W., Williams T. B., O'Donoghue D., 2003, in Iye M., Moorwood A. F. M., eds, Proc. SPIE Conf. Ser. Vol. 4841, Instrument Design and Performance for Optical/Infrared Ground-Based Telescopes. SPIE, Bellingham, p. 1634

Lamb J. B., Oey M. S., Segura-Cox D. M., Graus A. S., Kiminki D. C., Golden-Marx J. B., Parker J. W., 2016, ApJ, 817, 113

Luo J. et al., 2021, ApJ, 911, 45

McBride V. A. et al., 2017, MNRAS, 467, 1526

NASA High Energy Astrophysics Science Archive Research Center (HEASARC), 2014, Astrophysics Source Code Library, record ascl:1408.004

Okazaki A. T., Negueruela I., 2001, A&A, 377, 161

Pecaut M. J., Mamajek E. E., 2013, ApJS, 208, 9

Scowcroft V., Freedman W. L., Madore B. F., Monson A., Persson S. E., Rich J., Seibert M., Rigby J. R., 2016, ApJ, 816, 49

Skowron D. M. et al., 2021, ApJS, 252, 23

Udalski A., Szymański M. K., Szymański G., 2015, Acta Astron., 65, 1

van den Eijnden J. et al., 2020, Astron. Telegram, 14193, 1

van den Eijnden J. et al., 2021, MNRAS, 507, 3899

van den Eijnden J., Degenaar N., Russell T. D., Hernández Santisteban J. V., Wijnands R., Miller-Jones J. C. A., Rouco Escorial A., Sivakoff G. R., 2019, MNRAS, 483, 4628

Vasilopoulos G., Zezas A., Antoniou V., Haberl F., 2017, MNRAS, 470, 4354

Vreeswijk P., Paterson K., 2021, Astrophysics Source Code Library, record ascl:2105.011

Willingale R., Starling R. L. C., Beardmore A. P., Tanvir N. R., O'Brien P. T., 2013, MNRAS, 431, 394

Zechmeister M., Kürster M., 2009, A&A, 496, 577

This paper has been typeset from a TEX/LATEX file prepared by the author.